Laser and Particle Beams (2001), *19*, 47–53. Printed in the USA.

Investigation of ultraintense femtosecond laser–plasma interactions through ω and 2ω imaging and spectroscopy

M. GALIMBERTI,[1,2,3] A. GIULIETTI,[1] D. GIULIETTI,[1,2,3] L.A. GIZZI,[1] PH. BALCOU,[4] A. ROUSSE,[4] AND J.PH. ROUSSEAU[4]

[1]Intense Laser Irradiation Laboratory, Istituto di Fisica Atomica e Molecolare, CNR, Area della ricerca, via Moruzzi, 1-56124, Pisa, Italy
[2]Dipartimento di Fisica, sezione INFM, Università degli studi di Pisa, via Bonarotti 2, 56100 Pisa, Italy
[3]Istituto Nazionale di Fisica Nucleare, Sezione di Pisa
[4]Laboratoire d'Optique Appliquée, ENSTA–Ecole Polytechnique, CNRS Unité Mixte de Recherches 7639, F-91761 Palaiseau, France

(RECEIVED 24 January 2000; ACCEPTED 5 February 2001)

Abstract

A laser–plasma interaction experiment was performed in order to match effective conditions for wake-field electron acceleration. A 30-fs pulse was made to interact with a preformed plasma generated via the exploding foil technique from a 1-μm-thick plastic film. The irradiance of the femtosecond pulse in the plasma was 10^{20} Wcm^{-2}. The interaction conditions were investigated via imaging and spectroscopy at the fundamental and the second harmonic of the laser frequency, both forward and backward. Our data clearly show that conditions suitable for electron acceleration are achieved close to the propagation axis and can be easily reproduced from shot to shot. In contrast, significant growth of instabilities occurs at the boundaries of the interaction region. These observations are consistent with a preliminary evidence of forward acceleration of high-energy electrons. Optical, X-ray, and γ-ray data obtained for different positions of the foil target with respect to the laser focal plane further support this promising scenario.

1. INTRODUCTION

Particle acceleration methods based on laser–plasma interactions have been suggested for more than 20 years (Tajima & Dawson, 1979). Up to now, significant results have been obtained (Gemillet *et al.*, 1999), and many laboratories are presently involved worldwide in theoretical, computational and experimental research programs devoted to the achievement of intense, collimated, highly energetic electron beams.

Among a number of different schemes considered so far, the laser wake-field acceleration (LWA) scheme (Gorbunov & Kirsanov, 1987) has become one of the most promising due to the recent availability of very powerful laser pulses lasting a few optical cycles. The simplest model of such a mechanism is based on the interaction of a pulse of duration τ with a uniform plasma whose density n_e allows resonant excitation of electron waves of period $T \approx 2\,\tau$. More accurate calculations (Leemans *et al.*, 1996) show that the optimum conditions also depend on the pulse temporal shaping; assuming an acceleration length dominated by diffraction (Rayleigh length), there is a maximum energy gain of a particle in the field of a Gaussian laser beam which is independent from the laser spot size. Higher gains can be achieved if the acceleration length exceeds the Rayleigh length, due to nonlinear and/or hydrodynamic phenomena, as beam trapping, self-channeling, or existing preformed channels. In these cases, another limit to the acceleration length is given by the dephasing length, which is of the order of λ_p^3/λ_0^2, where λ_p and λ_0 are the electron plasma and laser wavelength, respectively.

A crucial issue in obtaining high LWA gain is the production of a suitable plasma for an efficient interaction with the ultrashort laser pulse. The laser-driven exploding foil technique can provide plasmas of long scale length with rather controllable density profiles. Such plasmas can also be simulated in advance using hydrodynamic numerical codes and experimentally characterized in detail (Gizzi *et al.*, 1994*a*, 1994*b*; Borghesi *et al.*, 1996). Foil thickness and material, together with the laser parameters, are the essential input parameters in obtaining a plasma of the required peak density and scale length.

For the 30-fs (Gaussian in time) Ti–Sapphire laser pulse that we used in our experiment, the optimum plasma density is approximately (Leemans *et al.*, 1998) $n_e^* \approx 2 \times 10^{18}$ cm^{-3}. The basic idea of the experiment described here was to try to

Address correspondence and reprint requests to: Marco Galimberti, Istituto di Fisica Atomica e Molecolare, CNR, Area della ricerca, via Moruzzi, 1-56124, Pisa, Italy. E-mail: galimberti@ifam.pi.cnr.it

profit from the nanosecond pedestal to preform a plasma having a density of the order of the one estimated above over a suitable length.

2. EXPERIMENTAL SETUP

The experimental setup was designed for this purpose, taking into account the actual pedestal as measured experimentally. In fact, according to preliminary hydrodynamic numerical simulation (M. Borghesi, pers. comm.) with the available pedestal, a target consisting of a 1-μm-thick plastic foil was required to generate a plasma having (at the time of the arrival of the short pulse) a peak density along the pulse propagation axis of the order of 2×10^{18} el/cm^{-3}. Moreover simulations gave an indication that, due to pure hydrodynamics effects related to the pedestal intensity distribution on target, a weak density depression (channel) could be present on the axis at the time of the short pulse propagation.

The Ti:Sapphire laser at the "Salle Jaune" of Laboratoire d'Optique Appliquée operated at a wavelength of 0.815 μm and delivered up to 800 mJ on target in a 30-fs FWHM pulse. The linearly p-polarized beam was focused in a 5-μm (FWHM) diameter spot on a 1-μm-thick plastic (FORMVAR) foil target, by using an f/6 off-axis parabolic mirror, with an angle of incidence on target of 20°. The laser system was characterized by an amplified spontaneous emission (ASE) lasting approximately 10 ns that formed a "pedestal" to the main pulse. The measured contrast ratio, that is, the ratio between the power delivered in the femtosecond pulse and the one delivered by the ASE, was $\approx 10^6$. According to the results of previous experiments performed in the same interaction regime, this level of prepulse is above the threshold for early plasma formation. As discussed above, the target thickness was chosen in order to have a plasma of maximum electron density of about 2×10^{18} el/cm^{-3} at the time of the interaction with the femtosecond pulse.

The main diagnostic equipment was devoted to the detection of γ-ray emission from bremsstrahlung of accelerated electrons. When dealing with large fluxes of pulsed γ-ray radiation, as in our case, spectral information can be obtained by using several detectors whose sensitivities are optimized for different photon energies. We used four 24.5-mm diameter detectors with scintillators 12.5 mm, 25.4 mm, and 50.8 mm thick, coupled to photomultipliers (PMs). The detectors were shielded by the heavy background radiation by means of lead bricks, while the line of sight was filtered with layers of lead sufficiently thick to keep the PM signal below saturation. The detectors were placed 5 m away from the target and could be moved around the chamber to perform angular dependence measurements. The response of our detectors is characterized by a pulse with a rise time of the order of a few nanoseconds, set by the photomultiplier tube, and by a fall time of 230 ns, which is the decay time of the scintillator. The height of the pulse is a measure of the energy released by one or more photons in the scintillation crystal. The detectors had been calibrated, in the single photon regime, using emission lines from radioactive sources including the 511 KeV and 1274 KeV lines from ^{22}Na source and 898 KeV and 1836 KeV lines from a ^{88}Y source. According to this calibration the pulse height was found to be linearly dependent on the photon energy in this range.

Three optical detection channels were also activated to acquire additional information on the laser–plasma interaction process. In the first one, the interaction volume was imaged forward, that is, in the direction of the propagation of the laser pulse. In this direction we obtained both images and spectra on CCD cameras, alternatively, at the laser frequency and at the second harmonic of the laser frequency. The second channel operated in a similar way at the fundamental and the second harmonic frequency, but emitted at $-140°$ with respect to the laser propagation axis. In this way we obtained eight series of optical data (four for images and four for spectra), which enabled us to achieve the best acceleration conditions. Additional information on the interaction was provided by soft X-ray detectors, namely an X-ray CCD and a PIN diode, both located at about $+140°$.

The next section is devoted to a description of the optical data and Section 3 summarizes the results on the X-ray data. γ-ray data are introduced in Section 4 along with a discussion of their correlation with transmission and reflection of laser light, as well as with X-ray emission. The observed properties of the laser-plasma interaction and the preliminary evidence of efficient high-energy electron acceleration are discussed in the last section.

3. ω AND 2ω IMAGING AND SPECTROSCOPY

3.1. Forward data

The 30-fs pulse was transmitted through the preformed plasma with no significant changes in its cross-sectional intensity distribution or in its spectrum. On the other hand, the forward-emitted second harmonic radiation shows interesting spatial and spectral features.

A representative image of the transmitted pulse cross section taken forward is shown in Figure 1a. The cross section is slightly elongated in the direction perpendicular to polarization, with respect to the far field Gaussian pattern obtained without target. However, the global spot size is basically unchanged (≈ 10 μm). A weaker emission is also visible outside the main spot.

A completely different shape was obtained from forward imaging of the second harmonic sources in the same region, as shown in Figure 1b. These images typically show a double (sometime multiple) structure. The size of each structure is comparable with the focal spot size in the direction perpendicular to the polarization axis, but definitely smaller in the direction of the polarization axis.

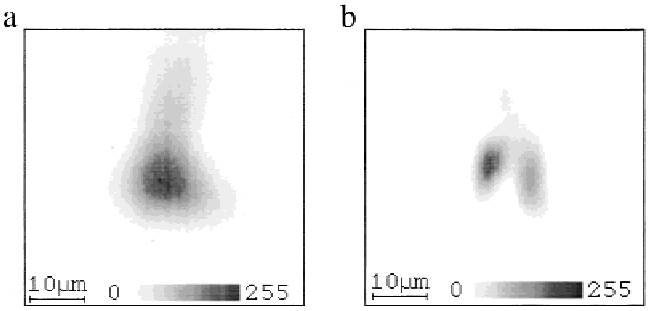

Fig. 1. Images of the transmitted laser pulse cross section (a) and the source of the forward emitted second harmonic light (b). The relative position of the two images cannot be stated.

The spectrum of the transmitted laser light, spatially resolved perpendicularly to the polarization axis, is shown in Figure 2a, where the lines M and m refer to the profiles shown in Figure 2b and Figure 2c, respectively. In the last two figures, the dotted curve is the spectrum of the unperturbed 30-fs laser pulse, which is clearly asymmetric, with the red side steeper than the blue one. The blue side is likely to be affected by the contribution of ASE radiation. In fact, the latter was found to be peaked at 790 nm in place of 820 nm of the main CPA pulse. It may be interesting to compare the unperturbed laser spectrum with the spectra obtained in the position of the main spot (M) and in the marginal position (m), respectively. In the M position, the main component of the spectrum is unshifted and narrowed, while tails appear in both blue and red sides. In the m position, all these features are confirmed except narrowing, and the red tail grows up in a peak.

The spectrum of the 2ω light emitted forward is shown in Figure 3. In this case, it was not possible to obtain spatially resolved spectra. The dotted curve (exactly peaked at $\lambda_0/2$) is the calculated spectrum of the "pure" second harmonic of the laser light generated in a nonlinear medium, and is plotted as a reference. There is evidence for a substantial red shift (420 nm compared to 410 nm) of the 2ω light respect to $\lambda_0/2$. Notice that the observed value of 420 nm corresponds very closely to the second harmonic of the red component of the spectrum of the laser light transmitted in marginal positions (Fig. 2c).

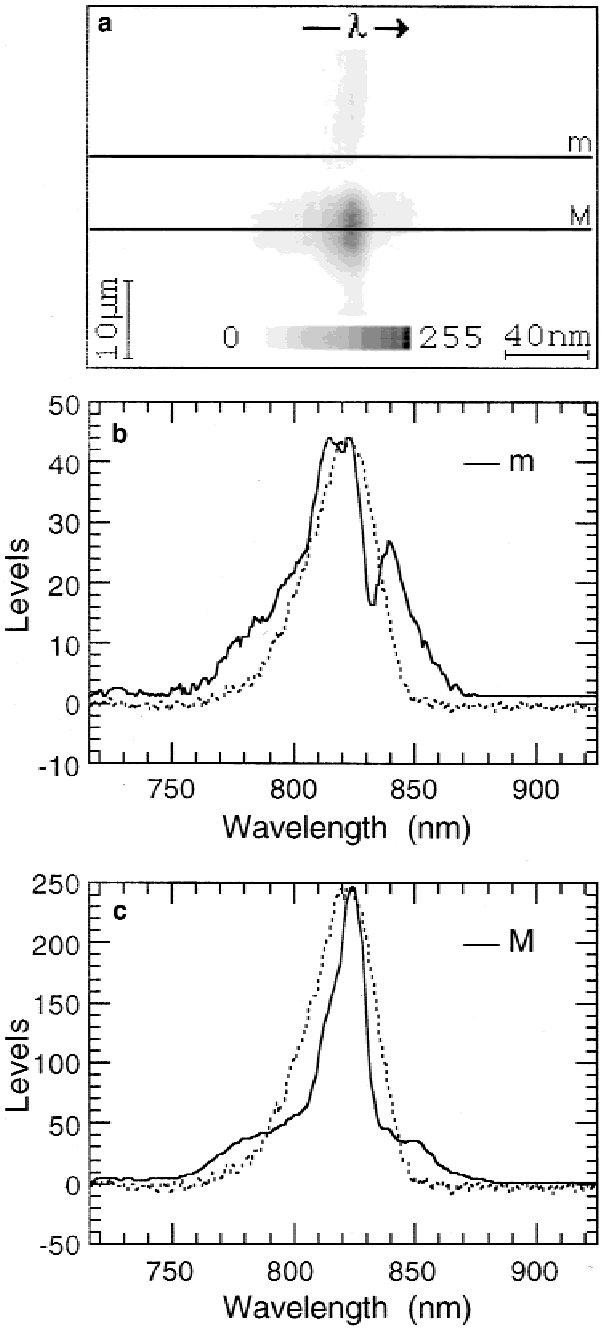

Fig. 2. Spatially resolved spectrum of the transmitted laser light, where lines m and M indicate the positions at which the two line-outs, m and M, are taken, respectively. The unperturbed spectrum of the femtosecond CPA laser is shown for reference (dotted curve).

3.2. Near-backward emission data (reflection)

The images obtained at $-140°$ from the propagation axis show complex structures both in the fundamental and in the 2ω light, extending spatially in a region much larger than the focal spot. Also the spectra are considerably shifted and broadened, particularly in the 2ω case.

The source of the laser light scattered at $-140°$ consists of a variable number of spots, generally located in an annular region of several tens of micrometers in width. The pattern resulting from these structures changes substantially shot by shot. An example of such a pattern is shown in Figure 4a. Also the 2ω sources emitting at $-140°$ are spread out from the center in separate structures, as shown in Figure 4b. In many cases, such structures are regularly modulated in space in the direction of laser propagation, as the upper feature of Figure 3b is. The modulations of that feature are clearly shown in Figure 4c.

A typical spectrum of the laser light scattered at $-140°$ is shown in Figure 5a. There is shift and broadening in the blue

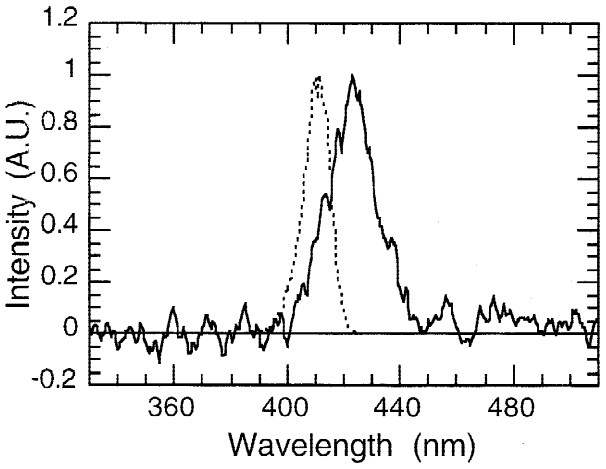

Fig. 3. Spatially integrated spectrum of the second harmonic light emitted forward. The dotted curve shows the calculated "pure" 2ω spectrum.

side with respect to the unperturbed laser spectrum, while the red-side limit of the spectrum is basically unchanged.

On the contrary, all the spectra of the 2ω light show a blue-shift limit very close to $\lambda_0/2$, while they extend towards the red for many tens of nanometers. Figure 5b shows one of these spectra. In this case, as for many other shots, the spectrum shows well separated, rather regularly spaced spectral peaks.

4. γ-RAY DATA

Four γ-ray detectors, equipped with three scintillator layers of different thicknesses have been used, as described in the setup description of Section 1. Due to the unexpectedly high γ-ray flux on detectors, very thick layers of lead had to be used to reduce the PM signals down to a working regime. In this configuration, lead acts as a simple, energy-independent attenuator and additional data is needed to obtain spectral properties of these γ-rays. A discussion of these issues is given in Section 5. Here we simply present some direct evidence coming from the data.

The first result concerns dependence of the γ-ray signal upon the thickness of the exploding foil target. As discussed above, the configuration we have chosen to optimize acceleration conditions was based upon a 1.0-μm thick target. Our measurements show that when thinner targets (0.1 μm) are used, the γ-ray signal goes below the detection threshold. In other words, the γ-ray signal shows a reduction of at least two orders of magnitude compared to the case of interaction with a 1.0-μm-thick target. The second evidence is the dramatic decrease of the γ-ray signal when the 1.0-μm foil is moved out of the best focus of the laser focusing optics. This effect will be shown in the next section.

Finally, as shown in Figure 6, a well-defined angular distribution of the γ-ray emission was found in our experiment, strongly peaked along the direction of the laser propagation axis and an angular spread of $\Theta(\mathrm{FWHM}) = 42.5 \pm 0.4°$.

5. FOCAL SCAN DATA

A focal scan was performed by changing the target position along the laser propagation axis in order to investigate the effect of the focusing conditions on measured quantities, including transmitted and reflected laser light and X-ray and γ-ray emission. The plots shown in Figure 7 show a clear dependence of the measured quantity of the target position. A minimum (or a maximum) is found in the proximity of the best focus while a clear change takes place for distances from the nominal best focus comparable with or greater than the Rayleigh length of the laser focusing optics. In other words, all of the phenomena studied appear to be correlated to the focusing conditions, γ-ray data were obtained at two angles of detection and in both cases a maximum is found in the range of target positions for which maximum transmission (and minimum reflection) of laser energy occurs.

X-ray emission was measured with two different kinds of detectors, located at about 140° from the laser propagation, a cooled CCD, and a PIN diode. Data from both detectors consistently show that the X-ray yield is minimum close to the best focus and increases when the target is out of the Rayleigh region. A simple *shadow* test performed on the CCD detector to determine the extent of the X-ray source showed, however, that no localized X-ray source exists. It is most likely, therefore, that the X-ray radiation was generated by secondary emission from the chamber walls irradiated by high energy electrons.

6. DISCUSSION AND CONCLUSION

The data obtained in this experiment provide relevant information on the interaction conditions in order to assess their suitability for laser wake-field acceleration. The short pulse is transmitted without significant modification of its cross-sectional intensity distribution. This is consistent with the CPA propagation in low density plasma channel, which, according to preliminary numerical simulations, is expected to be formed by the ASE. A small fraction of the laser light is reflected or scattered at large angles, basically from regions which are marginal with respect to the propagation channel.

The optical data show that the marginal regions are quite unstable. The second harmonic emission is a signature of such instability. Second harmonic emission has already proven to be a useful tool to investigate ultrashort laser interactions (Gizzi *et al.*, 1996). Second harmonic emitted forward originates mainly from the boundary of the transmission channel, and is generated by a small fraction of the main pulse. This explains the clear difference in second harmonic images and spectra from the ones of the transmitted laser pulse.

The spectrum of the transmitted laser light has two interesting tail-like features; the blue one is mostly due to the residual contribution of ASE; the red one can be attributed to self-phase-modulation (SPM) due to the fast channel rar-

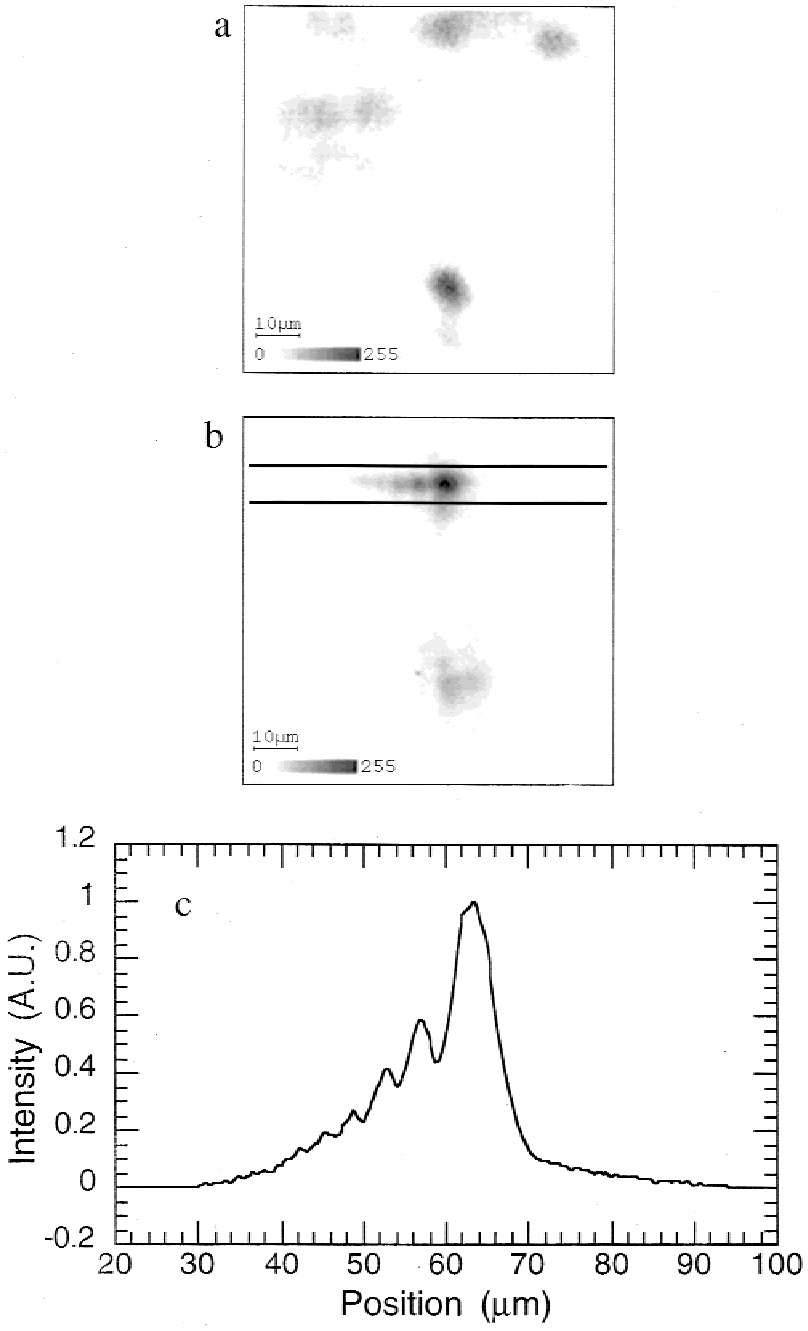

Fig. 4. Images of the sources of −140° scattered laser light (a) and the sources of −140° emitted second harmonic light (b). (c) The line-out of the selected part of (b).

efaction and is more evident at the channel boundary. It is interesting to compare these spectra with the spectra of the transmitted laser light obtained in a previous experiment (Giulietti *et al.*, 1997). In that case, there was no preformed plasma and the femtosecond pulse interacted directly with the foil. A net blue shift of the spectrum was observed in that case, and explained in terms of SPM due to ultrafast ionization. The spectrum of SH emitted forward can be strictly connected with the marginal propagation of a minor part of the short pulse at the boundary of the channel, as it is exactly peaked at $\lambda/2$ of the red component of the laser pulse after propagation.

The optical data obtained at −140°, both at the fundamental and the second harmonic frequency show signatures of scattering from an unstable region, marginal with respect to the channel. This is also proved by the unreproducible fragmentation of the scattering sources. The spectral broadening towards the blue of the scattered laser light can be again the signature of fast ionization of colder marginal regions of the plasma.

Special attention should be devoted to the second harmonic data collected at −140°. In fact, some regular spatial modulations of the sources, as well as spectra very broadened toward the red, suggests that second harmonic could be

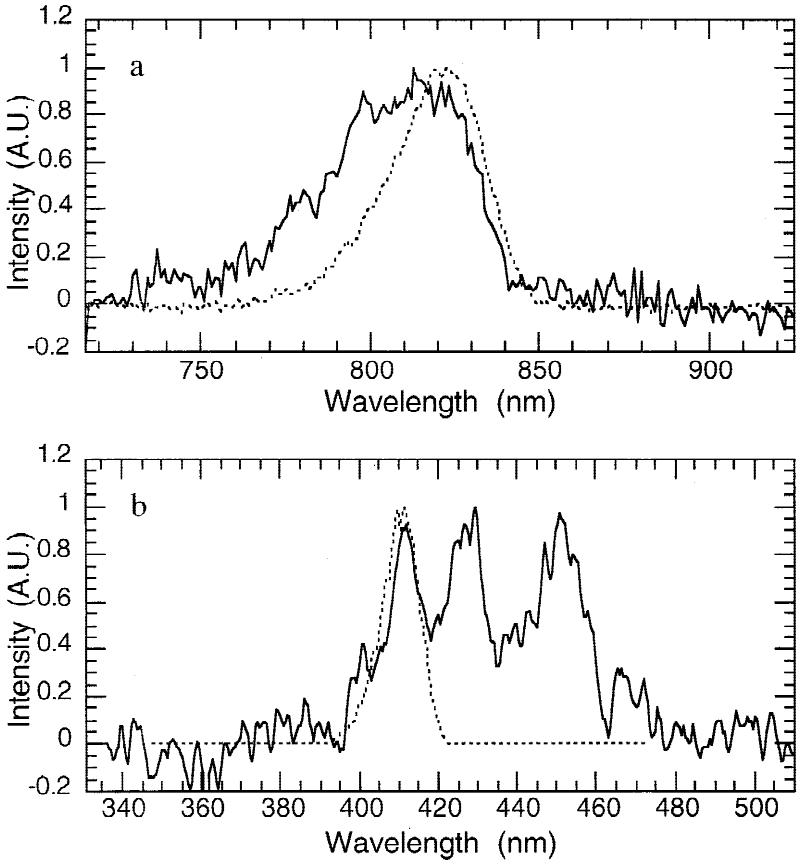

Fig. 5. Spectra of the $-140°$ scattered laser light, compared with the unperturbed spectrum of the femtosecond CPA laser (dotted curve) (a); and the $-140°$ emitted second harmonic light compared with the calculated "pure" 2ω spectrum (dotted curve) (b).

generated by Raman back-scattered laser light (the latter could be masked in the spectra at the fundamental frequency by some more efficient source of laser scattering). We point out here that these features could be the evidence of the creation and propagation of solitons in the plasma as predicted by some theoretical studies and numerical simulations (Bulanov *et al.*, 1995).

Apart from the interesting unstable marginal region, the regular propagation of the main spot is consistent with the observation of an intense forward gamma-ray emission generated by interaction (bremsstrahlung) of accelerated electrons with the vacuum chamber walls. The observed angular distribution of the γ-ray emission and its dramatic reduction when the target is moved out of focus are consistent with a

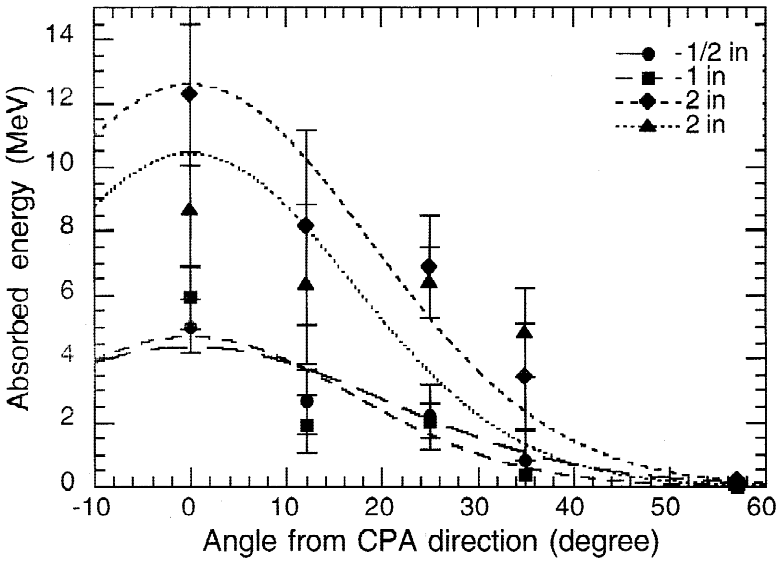

Fig. 6. Angular distribution of the γ-ray emission; different curves refer to different scintillator thicknesses (see text).

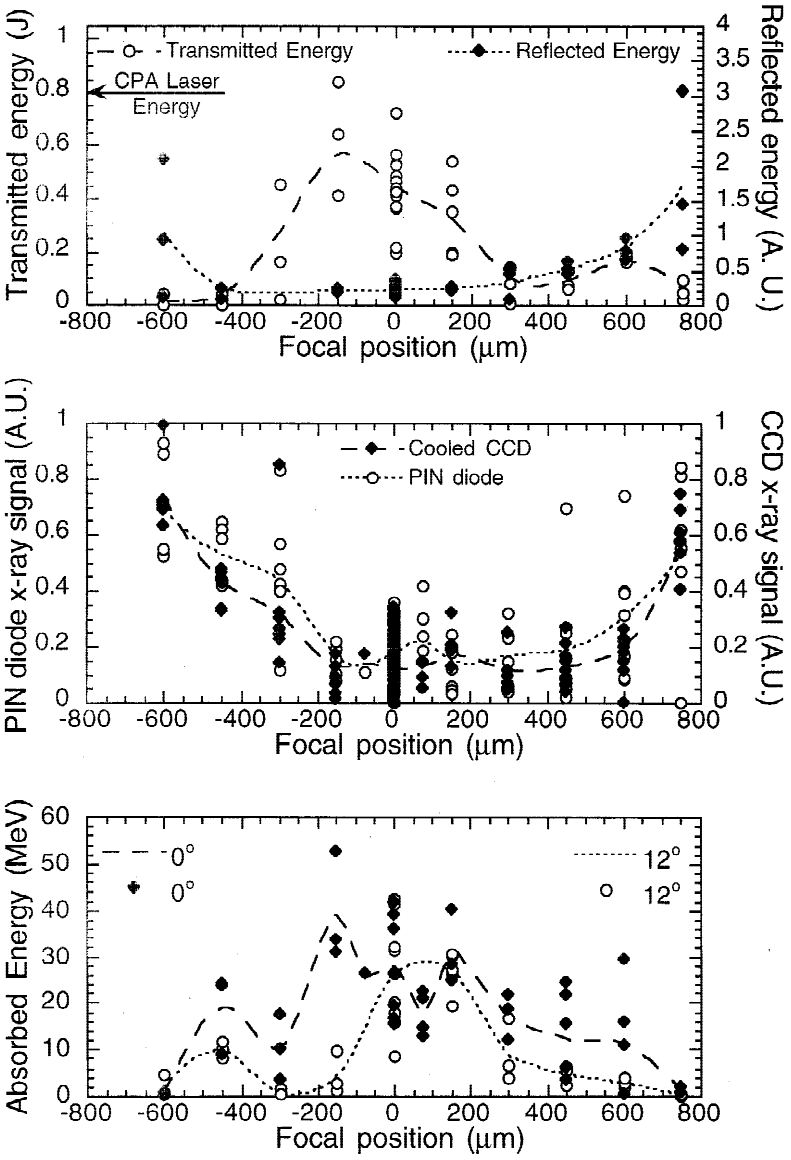

Fig. 7. Experimental data versus target distance from the focal plane: (top) Transmitted and reflected laser energy; (middle) X-ray energy collected by the cooled CCD and PIN diode, respectively; (bottom) γ-ray energy collected at 0 and 12°.

resonant wake-field acceleration. Monte Carlo simulations (Galimberti, 2000) compared to our γ-ray measurements indicate that a population of fast electron with energies of many tens of megaelectronvolts is generated.

Moreover, the X-ray data show that, when the target is out of focus (lower laser irradiance, higher plasma density), the collimated high energy electron beam turns into lower energy, uncollimated electrons impinging the chamber wall, and producing an extended source of X rays.

ACKNOWLEDGMENTS

This work was partially supported by the European Community within the scheme of Access to Large Facilities of the TMR Programme. The authors would like to thank Alessandro Barbini from IFAM and George Grillon from LOA for their invaluable technical support and their contribution to the solution of many difficult experimental problems. The authors are very grateful to Antonella Rossi for her very accurate foil target preparation.

REFERENCES

Borghesi, M. *et al.* (1996). *Phys. Rev. E* **54**, 6769.
Bulanov, S.V. *et al.* (1995). *Plasma Phys. Rep.* **22**, 600.
Galimberti, M. (2000). IFAM-Report, 05/122000.
Gemillet, L. *et al.* (1999). *Phys. Rev. Lett.* **83**, 5015.
Giulietti, D. *et al.* (1997). *Phys. Rev. Lett.* **79**, 3194.
Gizzi, L.A. *et al.* (1994*a*) *Phys. Rev. E* **49**, 5628.
Gizzi, L.A. *et al.* (1994*b*). *Phys. Rev. E* **50**, 4266.
Gizzi, L.A. *et al.* (1996). *Phys. Rev. Lett.* **76**, 2278.
Gorbunov, L.M. & Kirsanov, V.I. (1987). *Sov. Phys. JETP* **66**, 290.
Leemans, W.P. *et al.* (1996). *IEEE Trans. Plasma Sci.* **24**, 331.
Leemans, W.P. *et al.* (1998). *Phys. Plasmas* **5**, 1615.
Tajima, T. & Dawson, J.M. (1979). *Phys. Rev. Lett.* **43**, 267.